# Estimating Daytime Planetary Boundary Layer Heights over a Valley from Rawinsonde Observations at a Nearby Airport: An Application to the Page Valley in Virginia, United States

TEMPLE R. LEE* AND STEPHAN F. J. DE WEKKER

*Department of Environmental Sciences, University of Virginia, Charlottesville, Virginia*

(Manuscript received 15 October 2015, in final form 17 December 2015)

ABSTRACT

The planetary boundary layer (PBL) height is an essential parameter required for many applications, including weather forecasting and dispersion modeling for air quality. Estimates of PBL height are not easily available and often come from twice-daily rawinsonde observations at airports, typically at 0000 and 1200 UTC. Questions often arise regarding the applicability of PBL heights retrieved from these twice-daily observations to surrounding locations. Obtaining this information requires knowledge of the spatial variability of PBL heights. This knowledge is particularly limited in regions with mountainous terrain. The goal of this study is to develop a method for estimating daytime PBL heights in the Page Valley, located in the Blue Ridge Mountains of Virginia. The approach includes using 1) rawinsonde observations from the nearest sounding station [Dulles Airport (IAD)], which is located 90 km northeast of the Page Valley, 2) North American Regional Reanalysis (NARR) output, and 3) simulations with the Weather Research and Forecasting (WRF) Model. When selecting days on which PBL heights from NARR compare well to PBL heights determined from the IAD soundings, it is found that PBL heights are higher (on the order of 200–400 m) over the Page Valley than at IAD and that these differences are typically larger in summer than in winter. WRF simulations indicate that larger sensible heat fluxes and terrain-following characteristics of PBL height both contribute to PBL heights being higher over the Page Valley than at IAD.

## 1. Introduction

Turbulent mixing processes within the planetary boundary layer (PBL) govern the exchange of heat, moisture, momentum, and aerosols between Earth's surface and the overlying free atmosphere (e.g., Stull 1988). The PBL height represents the maximum height to which these turbulent mixing processes occur. On diurnal time scales, the PBL height is often highest in the afternoon. Thus, the afternoon PBL height is vital to describing the vertical mixing of trace gases and pollutants in studies of air-pollution dispersion (e.g., Dabberdt et al. 2004). Whereas the role of PBL height in trace-gas variability over flat terrain is understood well (e.g., Pochanart et al. 2003; Volz-Thomas et al. 2003; Elansky et al. 2007; Popa et al. 2010; Sahu et al. 2011), this knowledge is limited for mountainous regions. Previous studies have suggested that air masses representative of background concentrations are sampled at mountaintops when the valley PBL height remains well below the mountaintop, whereas local-to-regional pollutant sources affect the mountaintop trace-gas variability when the valley PBL height reaches or exceeds the mountaintop height (e.g., Raatikainen et al. 2014). Acquiring this information is vital if mountaintop trace-gas measurements are used in applications that require background trace-gas measurements, for example, air-chemistry models and inverse carbon-transport models.

Estimates of PBL heights can come from many different platforms, including wind profilers, lidars, sodars, tethered balloons, masts, rawinsonde observations, aircraft observations (e.g., Clifford et al. 1994; Nyeki et al. 2000; Pal et al. 2014), and, more recently, spaceborne lidars (Winker et al. 2007; Jordan et al. 2010). Each of these platforms has its own distinct advantages and

* Current affiliation: University of Maryland Earth System Science Interdisciplinary Center, and NOAA ARL Atmospheric Turbulence and Diffusion Division, Oak Ridge, Tennessee.

*Corresponding author address*: Dr. Temple R. Lee, NOAA Atmospheric Turbulence and Diffusion Division, 456 S. Illinois Ave., Oak Ridge, TN 37830.
E-mail: temple.lee@noaa.gov

DOI: 10.1175/JAMC-D-15-0300.1

disadvantages [see Seibert et al. (2000) for more details]. Of these platforms, rawinsonde observations, typically made at airports, are well suited for long-term daily and subdaily estimates of PBL heights because they are made at least 2 times per day at hundreds of sites worldwide. Thus, rawinsondes observations have been used to develop climatological descriptions of PBL height on continental to global scales (e.g., Holzworth 1964; Seidel et al. 2010; Liu and Liang 2010; Seidel et al. 2012; Wang and Wang 2014). Rawinsonde observation platforms are unevenly distributed globally, however, and are hundreds of kilometers apart in many areas. If rawinsonde observations or other observations of PBL height are unavailable for a particular location of interest, one approach is to use PBL heights obtained from the nearest sounding station as a proxy (e.g., Hondula et al. 2013). Another approach is to use geostatistical interpolation procedures (e.g., Cressie 1993)—for example, kriging with external drift (Kretschmer et al. 2013; Kretschmer et al. 2014)—to spatially interpolate rawinsonde PBL heights to data-sparse regions. These approaches neglect the physical processes affecting PBL-height spatial variability that occur between individual point observations of PBL height. Differences over a scale of hundreds of kilometers (i.e., the typical distance between rawinsonde stations) can be several hundred meters (e.g., Bianco et al. 2011; Bohnenstengel et al. 2011; Xie et al. 2013). Spatial differences in sensible heat flux (SHF) that are due to, for example, soil moisture (e.g., Avissar and Schmidt 1998; Segal et al. 1988; Desai et al. 2006; Ma et al. 2011) or land use (e.g., Bianco et al. 2011) are often cited as main drivers of spatial PBL-height differences. In complex terrain, thermally and dynamically driven flows also affect spatial PBL-height differences (e.g., Kossmann et al. 1998; De Wekker 2002; Bianco et al. 2011; De Wekker and Kossmann 2015). Accounting for these processes is important for understanding the spatial variability of PBL heights between point observations. Another approach for obtaining PBL-height estimates is to use reanalysis or forecasting products, which assimilate rawinsonde observations and cover, at least partially, the physical processes that drive spatial variations in PBL height. For example, the High-Resolution Rapid Refresh Model provides estimates of PBL height at 3-km spatial scales (e.g., Olson and Grell 2014) and the Weather Research and Forecasting (WRF) Model can generate PBL-height estimates at 1-km spatial scales (e.g., Xie et al. 2012). Even so, in regions with complex or mountainous terrain, PBL-height estimates at this high resolution may not always be valid because of subgrid PBL-height spatiotemporal variability (e.g., Kalthoff et al. 1998; Kossmann et al. 1998). Furthermore, models used to generate these PBL-height estimates can have difficulty resolving atmospheric processes at these spatial scales, particularly over mountainous terrain (e.g., Zhong and Chow 2013).

In the current paper, we develop an approach to estimate PBL heights that uses a combination of PBL heights obtained from a sounding station and from reanalysis products. We demonstrate our approach for the estimation of afternoon PBL heights over the Page Valley, located in the Blue Ridge Mountains in Virginia, although our approach could be used to estimate PBL heights at other nearby locations as well. Acquiring reliable PBL-height estimates over the Page Valley in particular, though, is vital for our application because the valley is located ~15 km upwind of a long-term mountaintop trace-gas monitoring site where select atmospheric trace gases have been continuously monitored since 2008 (e.g., Lee et al. 2012; Lee 2015). For the purpose of determining the degree to which the nearby mountaintop trace-gas measurements are affected by local-to-regional pollutant sources, we have hypothesized the importance of PBL height (Lee et al. 2015) and need reliable estimates thereof over the Page Valley. The sounding station nearest the Page Valley at which twice-daily rawinsonde observations are available is located at Dulles Airport (IAD) (38.98°N, 77.49°W; 87 m MSL), 90 km northeast of the Page Valley (Fig. 1a) in a suburban setting ~35 km northwest of Washington, D.C. Because of the regional topography, which is discussed in more detail in the next section, the Page Valley receives less rainfall annually than IAD does. We hypothesize that, despite the relatively close proximity of the Page Valley to IAD, PBL heights will be higher over the Page Valley than at IAD because of higher SHF and terrain height over the Page Valley than near IAD. To test this hypothesis, we first present our approach to obtain PBL-height estimates for the Page Valley from the IAD rawinsonde observations. We evaluate our approach with aircraft observations from IAD and rawinsonde observations from the Page Valley. We then investigate the underlying physical processes that are responsible for the PBL-height variability in this region by using output from the North American Regional Reanalysis (NARR) and simulations with WRF.

## 2. Site description

The Page Valley is oriented from south-southwest to north-northeast, is approximately 80 km long, on average is 10–15 km wide, and ranges in elevation from ~200 m MSL on its northern end to ~400 m MSL on its southern end. The Page Valley is part of the larger Shenandoah Valley and is separated from the rest of the

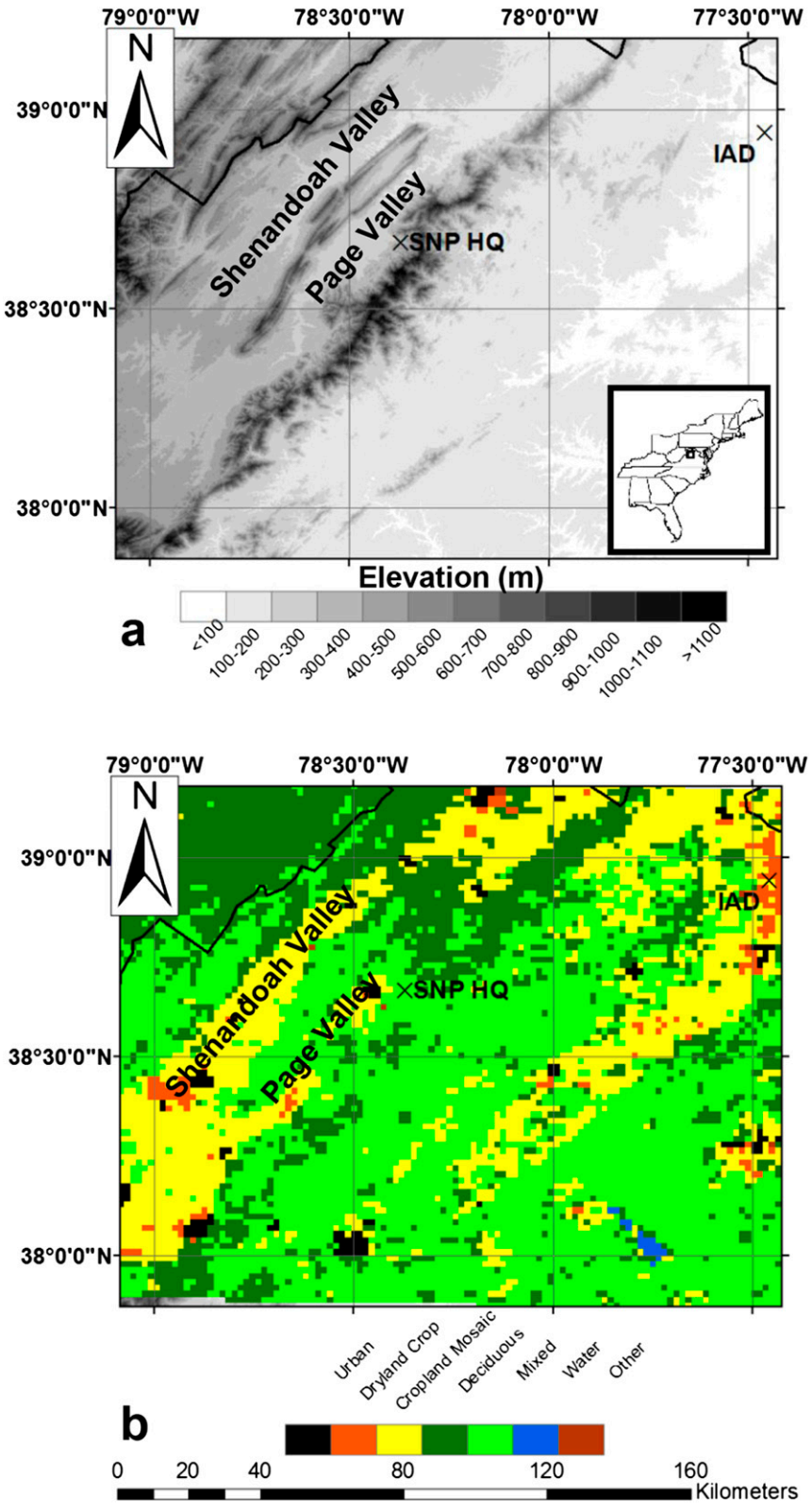


FIG. 1. (a) The regional topography (shaded) over the innermost WRF domain with the locations of SNP HQ and IAD (times signs) identified relative to the Page and Shenandoah Valleys; inset map at the bottom right shows the location of the study region, denoted by a black box, in the eastern United States. (b) The dominant land-use types (shaded). Elevation and land-use data are from the U.S. Geological Survey.

Shenandoah Valley by the Massanutten Mountains, which have a maximum elevation of ~800 m MSL. East of the Page Valley are the Blue Ridge Mountains with a ridgeline at 1000–1200 m MSL. The valleys are mostly rural and have a total population of approximately one million inhabitants (e.g., Davis et al. 2010).

The regional climate is humid subtropical at the lower elevations but is humid continental along and west of the Blue Ridge Mountains. Rainfall in the region is evenly distributed throughout the year (e.g., Lee et al. 2012, 2014a) but varies across the Blue Ridge Mountains. The Page Valley receives 85 cm of precipitation annually and is among the driest locations in Virginia. The ridgetops surrounding the Page Valley receive 135 cm of precipitation annually; locations east of the Blue Ridge Mountains, including the sounding station at IAD, receive approximately 105 cm (http://prism.oregonstate.edu; accessed 4 February 2015).

## 3. Datasets and models

### a. Valley rawinsonde observations

Rawinsonde observations have been made in the Page Valley during the Education in Complex Terrain Meteorology field experiment as a component of an undergraduate mountain meteorology course taught at the University of Virginia and of outreach activities with nearby high schools. Rawinsondes were launched from the Shenandoah National Park Headquarters (SNP HQ; 38.67°N, 78.37°W; 351 m MSL). SNP HQ (Fig. 1a) is located in a small basin approximately 1 km wide in the eastern part of the Page Valley and is separated from the rest of the Page Valley by a 100-m hill. In the this study, we used rawinsonde observations from 9 April 2009 and from 23 October 2010 for model evaluation, which we discuss in the appendix.

### b. Rawinsonde observations at IAD

Rawinsonde observations are made at IAD at 0000 UTC (1900 LST) and 1200 UTC (0700 LST). These observations are obtained from the University of Wyoming sounding archive (http://weather.uwyo.edu/upperair/sounding.html) and are used to calculate PBL heights over the period from 1 January 2009 to 31 December 2012 following the approach discussed in section 4a. Sounding observations are linearly interpolated every 100 m.

### c. Aircraft profiles

Vertical profiles of temperature and wind are also obtained from the Aircraft Communications Addressing and Reporting System (ACARS) dataset (https://madis.noaa.gov/madis_acars.shtml). The ACARS dataset, which is available for IAD from autumn 2009 through the present, is used for comparison with IAD PBL height in section 4b(1), as well as for model evaluation on select days. ACARS provides meteorological observations from aircraft during takeoffs and landings and has been used to estimate PBL heights over regions where PBL-height estimates are unavailable (e.g., Drüe et al. 2010; Yver et al. 2013). The advantage of the ACARS dataset in our study region is that it provides soundings that are closer to the time of maximum PBL height than can be provided by the 0000 UTC rawinsonde observations, which helps in evaluating our approach of estimating afternoon PBL height in the region.

### d. Surface observations

We evaluated our WRF simulations, described in section 3e, using surface meteorological observations from IAD and the Page Valley, as well as from Pinnacles and Big Meadows, which are two long-term mountaintop monitoring stations in the Blue Ridge Mountains (e.g., Lee et al. 2014a). In the Page Valley, meteorological observations are obtained from a MesoWest fire-weather station (e.g., Horel et al. 2002) at SNP HQ, which has hourly measurements of temperature and relative humidity at 2 m above ground level (AGL), wind speed and direction at 6.1 m AGL, incoming shortwave radiation, and precipitation.

### e. Gridded PBL-height products

Gridded PBL heights can come from reanalysis products—for example, NARR (Mesinger et al. 2006)—as well as from numerical weather prediction (NWP) models—for example, the European Centre for Medium-Range Weather Forecasts (ECMWF) model, the North American Mesoscale Forecast System (NAM), and the Rapid Update Cycle. Although NWP models have a higher spatial resolution than reanalysis products, NWP models are based on forecasts, but reanalysis products are forecasts that are corrected a posteriori using surface and upper-air observations. For this reason, output from coarser-resolution reanalysis products has better agreement with observations than does output from higher-resolution NWP models (e.g., Yver et al. 2013). Therefore, we use the reanalysis product NARR to help to quantify the regional spatiotemporal variability in PBL height. We also discuss comparisons with other reanalysis products—for example, the National Centers for Environmental Prediction (NCEP) Climate Forecast System Reanalysis (CFSR; e.g., Saha et al. 2010)—and with higher-resolution forecast products—for example, the NAM.

NARR assimilates boundary conditions from the NCEP–U.S. Department of Energy global reanalysis,

the NCEP Eta Model, and surface and rawinsonde observations to generate meteorological fields at a 32-km resolution over North America. NARR has 29 vertical levels, 13 of which are below 3000 m (Mesinger et al. 2006). NARR output is available at a 3-h temporal resolution daily at 0000, 0300, 0600, 0900, 1200, 1500, 1800, and 2100 UTC over North America and is available online (http://ftp.cdc.noaa.gov/NARR). NARR outputs PBL heights at a 32-km resolution. These PBL heights are computed on the basis of vertical profiles of turbulent kinetic energy (TKE) calculated using a level-2.5 Mellor–Yamada closure scheme (Janjić 1990). We compute PBL heights from the NARR meteorological fields ourselves using the $R_b$ method, discussed in section 4a, so that NARR PBL heights can be directly compared with the IAD rawinsonde PBL heights. At IAD, the 0000 UTC NARR-derived PBL heights computed using the TKE method correlate well with PBL heights computed in NARR using the $R_b$ method (correlation coefficient $r = 0.82$; significance level $p < 0.01$). The NARR PBL heights are approximately 500 m higher than the observed PBL heights at IAD during the selected time period, however.

### f. WRF simulations

We used the WRF Model (Skamarock et al. 2008) to investigate underlying physical processes responsible for the spatiotemporal PBL height variability in this region. We used three model domains with two-way nesting that had a horizontal grid spacing of 9, 3, and 1 km, respectively. The outermost domain encompassed most of the eastern United States, the second domain included the Mid-Atlantic region, and the innermost domain included the entire Page Valley and IAD. The size of the innermost domain was 150 km × 150 km. Our simulations had 84 vertical levels between the surface and the model top of 100 hPa, and the thickness of the vertical levels increased gradually with height. The five lowest sigma levels of 0.997, 0.995, 0.992, 0.990, and 0.987 corresponded to heights of approximately 19, 41, 56, 78, and 93 m AGL, respectively. Terrain and vegetation information were obtained from a U.S. Geological Survey dataset with a 1-km spatial resolution. Over the innermost domain, the majority (53%) of the vegetation was mixed deciduous forest, and the remainder was mostly deciduous forest (23%) and cropland (21%; Fig. 1b) and reflects the actual land use in the area as based on satellite imagery (not shown). NARR is used to supply the boundary conditions for the simulations. In all WRF domains, we applied the Dudhia shortwave radiation scheme (Dudhia 1989), the Rapid Radiative Transport Model longwave scheme (Mlawer et al. 1997), the WRF 3-class simple ice microphysics scheme (Hong et al. 2004), the Kain–Fritsch cumulus scheme (Kain and Fritsch 1990) in the two outermost domains, and the Pleim–Xiu land surface model (LSM), which includes a surface model to describe soil moisture and evapotranspiration coupled with a nonlocal asymmetric convection model (Xiu and Pleim 2001). We used the Pleim–Xiu LSM because simulations using this LSM agreed better with regional observations than did simulations using the more common Noah LSM (Lee et al. 2014b).

We investigated the model sensitivity to a selection of PBL parameterization schemes commonly used in WRF. Different PBL schemes make varying assumptions about the transport of heat, moisture, and momentum between Earth's surface and the overlying atmosphere. In this study, we investigated the spatiotemporal PBL-height variability using two local PBL parameterization schemes: the Mellor–Yamada–Janjić (MYJ) scheme (Janjić 1990) and the Mellor–Yamada–Nakanishi–Niino level-2.5 (MYNN2) scheme (Nakanishi and Niino 2009) as well as two nonlocal PBL schemes: the Yonsei University (YSU) scheme (Hong et al. 2006) and the total energy mass flux (TEMF) scheme (Angevine et al. 2010). The MYNN2 scheme is newer than the MYJ scheme and improves some of its weaknesses—for example, slow daytime PBL growth (e.g., Sun and Ogura 1980)—by incorporating more-realistic diagnostic equations for turbulent length scale (Nakanishi and Niino 2009). The YSU PBL scheme is a first-order closure scheme that uses a nonlocal gradient adjustment term (e.g., Hong et al. 2006; Xie et al. 2012). The TEMF scheme is a 1.5-order closure scheme that describes vertical mixing by computing eddy diffusivity from the sum of turbulent kinetic and turbulent potential energy (Angevine et al. 2010). We performed WRF simulations for two days with multiple afternoon rawinsonde observations from the Page Valley: 9 April 2009, which is a day with a deep afternoon PBL, and 23 October 2010, which is a day with a shallow afternoon PBL. Although some PBL parameterization schemes explicitly calculate PBL heights, we computed PBL heights from the model output using the $R_b$ method, described in section 4, for a consistent comparison of PBL heights using different parameterization schemes.

## 4. Methods

### a. PBL-height determination

Many different methods that are based on various criteria exist to determine PBL heights from rawinsonde observations, including the parcel method (e.g., Seibert et al. 2000), elevated inversion depth (e.g., Holzworth

1964; Seidel et al. 2012), humidity gradients (e.g., von Engeln and Teixeira 2013), refractivity gradients (e.g., Seidel et al. 2010), maximum potential temperature gradient (e.g., Stull 1988; Seidel et al. 2010), and the bulk Richardson, or $R_b$, method (Vogelezang and Holtslag 1996) [see Seidel et al. (2010) for a review]. Although the different methods yield the same seasonal cycle in PBL height, the median difference in daytime PBL height among the methods for all sites within a global radiosonde network is 440 m, and the interquartile range is from 210 to 750 m (Seidel et al. 2010). Of these methods, the $R_b$ method has been shown to be most suitable for identifying PBL heights because it determines PBL height as a function of both buoyancy-driven and mechanically driven turbulence and also it is not strongly dependent on the vertical resolution of the soundings (e.g., Seidel et al. 2012). For these reasons, we used the $R_b$ method and computed the $R_b$ profile using the following equation:

$$R_b = \frac{(g/\theta_{vs})(\theta_{vz} - \theta_{vs})(z - z_s)}{(u_z - u_s)^2 + (v_z - v_s)^2 + bu_*^2}. \quad (1)$$

In Eq. (1), $g$ is the gravitational acceleration; $\theta_v$ is the virtual potential temperature; $z$ is the height; $u$ and $v$ are the zonal and meridional wind components, respectively; $b$ is a constant; and $u_*$ is the surface friction velocity. The subscripts $s$ and $z$ denote values at the surface and values at height $z$, respectively. Following Seidel et al. (2012), we ignored surface frictional effects. We also set $\theta_{vs}$ to the value at the first measurement height, which is typically 2 m AGL. Because surface winds are not reported in rawinsonde observations and since winds are typically weak at 2 m AGL, we used 0 m s$^{-1}$ for the surface winds, which is a practice consistent with many previous studies (e.g., Menut et al. 1999; Seidel et al. 2012; Korhonen et al. 2014; Zhang et al. 2014). In each $R_b$ profile, we scanned upward from the surface and determined the first height $z$ at which $R_b$ exceeded a critical threshold $R_c$, and then we linearly interpolated between $z$ and $z - 1$ (i.e., the height one level below $z$) to determine the PBL height. Following the procedure used in previous studies (e.g., Vogelezang and Holtslag 1996; Seidel et al. 2012), we set $R_c$ to 0.25.

### b. *Approach to estimate PBL height over the Page Valley*

We used IAD-sounding observations and NARR output to estimate daytime PBL heights over the Page Valley. We first estimated the afternoon PBL height from the 0000 UTC IAD sounding and compared these PBL heights with afternoon NARR PBL heights. We then determined a correction that is based on physical processes that affect PBL heights in the region of interest, which we applied to the IAD sounding to determine PBL heights over the Page Valley.

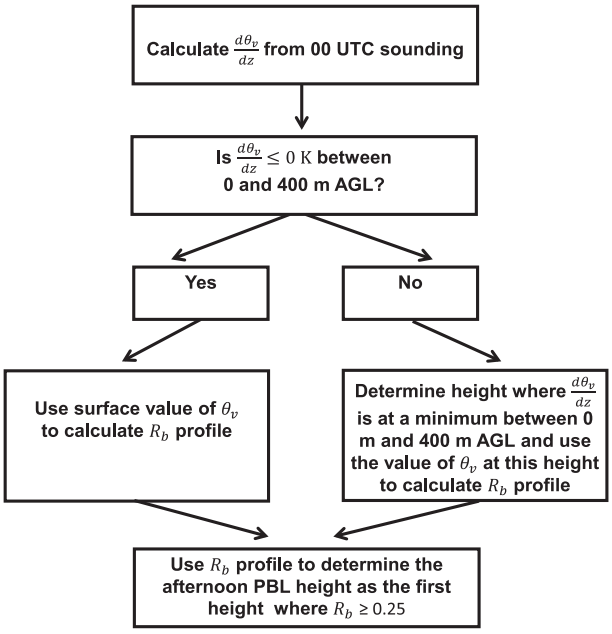


FIG. 2. Flowchart summarizing our approach to estimate afternoon PBL heights from 0000 UTC rawinsonde observations at IAD.

#### 1) DETERMINING AFTERNOON PBL HEIGHT FROM IAD RAWINSONDE OBSERVATIONS

In the eastern United States, 0000 UTC is equal to 1900 LST. For this reason, soundings at IAD are after local sunset between late August and late April. Near-surface cooling causes the formation of a near-surface stable layer around sunset. The formation of this stable near-surface layer complicates afternoon PBL-height determination (e.g., Wang and Wang 2014) and results in significant underestimates in afternoon PBL height in this region of the United States. To obtain reliable estimates of afternoon PBL height from the IAD-sounding observations, we developed an approach, summarized in Fig. 2, to remove the effect that this stable layer has on the determination of the afternoon PBL height. We computed the $\theta_v$ gradient, $d\theta_v/dz$, between each interpolated level below 500 m MSL (400 m AGL). If $d\theta_v/dz \le 0$, then we used the surface value of $\theta_v$ in Eq. (1) to calculate $R_b$. If $d\theta_v/dz > 0$, then we scanned upward to 500 m MSL in the profile, and used the value of $\theta_v$ in Eq. (1) at the height at which $d\theta_v/dz$ is at a minimum. Our choice of 500 m MSL was based on a presumed minimum depth of the afternoon PBL for this region. If $d\theta_v/dz > 0$ at each level between the surface and 500 m MSL, then we used the value of $\theta_v$ at 500 m

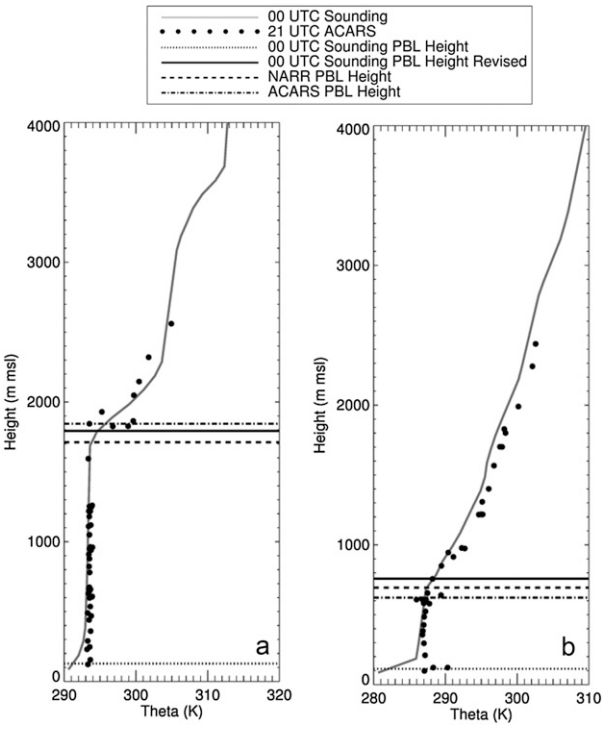


FIG. 3. Application of our afternoon PBL-height-detection approach to two IAD soundings from autumn 2010: (a) 1900 LST 1 Oct 2010 and (b) 1900 LST 11 Nov 2010. The dark-gray curve is the IAD sounding; black dots are a midafternoon (1500 LST) ACARS-derived $\theta$ sounding within a 0.25° × 0.25° box (approximately 28 km × 28 km) centered on IAD; the horizontal dotted line is the PBL height determined from the IAD sounding without applying our approach to remove the near-surface stable layer; the horizontal solid line is the PBL height determined from the IAD sounding with the application of our approach; the horizontal dashed line is the PBL height determined from NARR; the horizontal dash–dotted line is the PBL height determined from the ACARS profile. In all cases, PBL height is calculated using the $R_b$ method. Because moisture measurements are unavailable in the ACARS profiles at IAD, we assume that $\theta_v \approx \theta$.

MSL in Eq. (1). We set $u_s = v_s = 0\,\mathrm{m\,s^{-1}}$. Sensitivity tests (not shown), in which we varied the presumed minimum depth of the afternoon PBL between 400 and 600 m MSL, indicated that our results are not significantly affected by the choice of this threshold.

We demonstrate the above approach using rawinsonde data on two days in autumn of 2010. Radiative near-surface cooling led to the formation of a near-surface stable layer in the 0000 UTC sounding on 1 October 2010 and on 11 November 2010. Using surface values of $\theta_v$ yielded PBL heights of 128 and of 113 m MSL, respectively (Fig. 3). These values do not agree with the afternoon (2100 UTC) NARR PBL heights on these days, which were 1712 and 694 m MSL, respectively, and are unrealistic values for afternoon PBL height over this region of the United States (e.g., Aneja et al. 2000). When we applied our approach to the rawinsonde observations, we found revised PBL heights from the rawinsonde observations of 1781 and 801 m MSL, respectively. These PBL heights were <150 m different from afternoon PBL heights determined from NARR and from the afternoon ACARS observations on these days.

Improvements in afternoon PBL heights from the IAD rawinsonde observations were further evident when we compared PBL heights over the entire 4-yr period of interest. Without applying our approach, the correlation between the 0000 UTC IAD rawinsonde observations and afternoon (2100 UTC) NARR PBL height was $r = 0.40$ ($p < 0.01$). The mean and standard deviation of the difference between the IAD rawinsonde and NARR PBL height were 255 and 639 m, respectively, with the rawinsonde PBL height lower than the NARR PBL height. Applying our approach improved the correlation to $r = 0.56$ ($p < 0.01$) and reduced the mean difference and standard deviation so that the rawinsonde PBL height was 72 ± 479 m lower than the NARR PBL height. Important to note, though, is that our approach does not account for changes in PBL height between 2100 and 0000 UTC, in particular by subsidence, which can result in PBL-height decreases of 200 m between the midafternoon and early evening (e.g., Blay-Carreras et al. 2014). The potential errors caused by subsidence are less than the standard deviations in the PBL-height differences between the observed IAD PBL height and NARR PBL height, however, which were reduced from 639 to 479 m with the application of our approach. These relatively large standard deviations occurred because, in some cases, there are small $R_b$ and $\theta_v$ vertical gradients. When these gradients are small, the PBL height is not well defined (e.g., von Engeln et al. 2003). A poor relationship between rawinsonde observations and reanalysis output consequently exists in these cases. The Pearson correlation coefficient $r$ is lowest ($r = 0.29$; $p < 0.01$) and mean absolute errors are largest (mean NARR PBL height is 331 m higher than the IAD rawinsonde PBL height) during the summer but are smallest in the winter (Table 1). This seasonal dependence of NARR's performance has also been found by other researchers. For example, Schmid and Niyogi (2012) analyzed PBL heights for a 10-yr period in Oklahoma and found correlations between rawinsonde and NARR PBL height, computed using TKE vertical profiles, that ranged from 0.39 in spring to 0.58 in winter. Korhonen et al. (2014) found a correlation of 0.58 between rawinsonde and reanalysis PBL heights, obtained from the ECMWF model over South Africa and calculated using the $R_b$

TABLE 1. Pearson correlation coefficient, mean absolute error, and standard deviation of the difference between IAD rawinsonde and NARR PBL height computed using the $R_b$ method as a function of season [December–February (DJF), March–May (MAM), June–August (JJA), and September–November (SON)] for the period 1 Jan 2009–31 Dec 2012. The final row shows correlation coefficients between rawinsonde observations and NARR obtained from a 2002–10 study in Oklahoma (Schmid and Niyogi 2012). All values of $r$ are significant at the 0.01 confidence level.

| Relationship | Variable | DJF | MAM | JJA | SON |
|---|---|---|---|---|---|
| 0000 UTC rawinsonde vs NARR PBL height at IAD, with removal of near-surface stable layer | Correlation coef $r$ | 0.72 | 0.67 | 0.29 | 0.60 |
| | MAE, rawinsonde − NARR (m) | 4.8 | −111.1 | −331.0 | −189.1 |
| | Std dev, rawinsonde − NARR (m) | 358.0 | 429.2 | 601.5 | 423.7 |
| 0000 UTC rawinsonde vs NARR PBL height at IAD, with removal of near-surface stable layer and with a well-defined PBL height | Correlation coef $r$ | 0.78 | 0.76 | 0.59 | 0.67 |
| | MAE, rawinsonde − NARR (m) | 4.9 | −116.6 | −112.6 | −162.1 |
| | Std dev, rawinsonde − NARR (m) | 317.6 | 385.7 | 472.1 | 383.0 |
| Rawinsonde and NARR PBL height, Oklahoma (Schmid and Niyogi 2012) | Correlation coef $r$ | 0.58 | 0.39 | 0.43 | 0.56 |

method. In both studies, rawinsonde PBL heights were generally higher than reanalysis PBL heights, whereas we found the opposite. In comparison with these studies, studies in regions with mountainous terrain found lower correlations when evaluating model output, even when using higher-resolution models. For example, Ketterer et al. (2014) found that correlations ranged from 0.3 to 0.5 when comparing PBL heights calculated using the $R_b$ method in the Consortium for Small Scale Modeling (COSMO)-2 model, run at a 2.2-km resolution over the European Alps, with PBL heights obtained from wind profilers and ceilometers deployed in their study region. In their study, the observed PBL heights were generally higher than the model-derived PBL heights.

### 2) REMOVAL OF DAYS WITH POORLY DEFINED PBL HEIGHTS

Days for which PBL heights are not well defined caused uncertainty in determining PBL height differences between IAD and the Page Valley and needed to be removed. We followed von Engeln et al. (2003) and removed days characterized by the absence of a well-defined elevated-stable-layer inversion. To this end, we calculated NARR $\theta_v$ gradients every 100 m vertically for each sounding and removed cases with poorly defined elevated $\theta_v$ gradients, which we defined as those $< 1.0\,\mathrm{K}\,(100\,\mathrm{m})^{-1}$. Sensitivity tests (not shown) with values of this threshold between 0.5 and $2.0\,\mathrm{K}\,(100\,\mathrm{m})^{-1}$ indicated that the conclusions in this study were not significantly affected by our choice of this threshold. The removal of days that lacked a well-defined elevated stable layer reduced the number of days that we considered for further analysis by ~50%. The percentage of remaining cases varies seasonally: approximately 80% of the days remain in winter, and less than 20% of the days remain in summer (Table 2). The removal of these cases improved the relationship between IAD rawinsonde PBL heights and NARR PBL heights (cf. Table 1). Over the 4-yr period of interest, $r = 0.74$ ($p < 0.01$), and the mean difference was $1 \pm 378$ m. On seasonal time scales, $r$ ranged from 0.59 ($p < 0.01$) in summer to 0.78 ($p < 0.01$) in winter (Fig. 4), and mean monthly NARR PBL heights compared better to the IAD PBL heights (Fig. 5). This correlation was not biased by an unequal number of cases in the different seasons. Underestimates of PBL heights in NARR occurred most often on days with PBL heights that were higher than ~1500 m and were caused by a NARR cool bias of 2°–3°C throughout the depth of the PBL (not shown). Because PBL heights are typically highest in late spring and summer, NARR's cool bias may explain the lower correlations between the NARR and IAD-sounding PBL heights in these seasons. Nonetheless, there are some days for which the IAD-sounding PBL height and NARR PBL height differed by more than 1000 m. These days occur in all seasons, as indicated by the

TABLE 2. Percentage and number of days with a well-defined elevated $\theta_v$ inversion as a function of season at IAD for 1 Jan 2009–31 Dec 2012.

| | Percentage (No.) of days with well-defined inversion |
|---|---|
| DJF | 79% (285) |
| MAM | 36% (131) |
| JJA | 13% (47) |
| SON | 47% (170) |

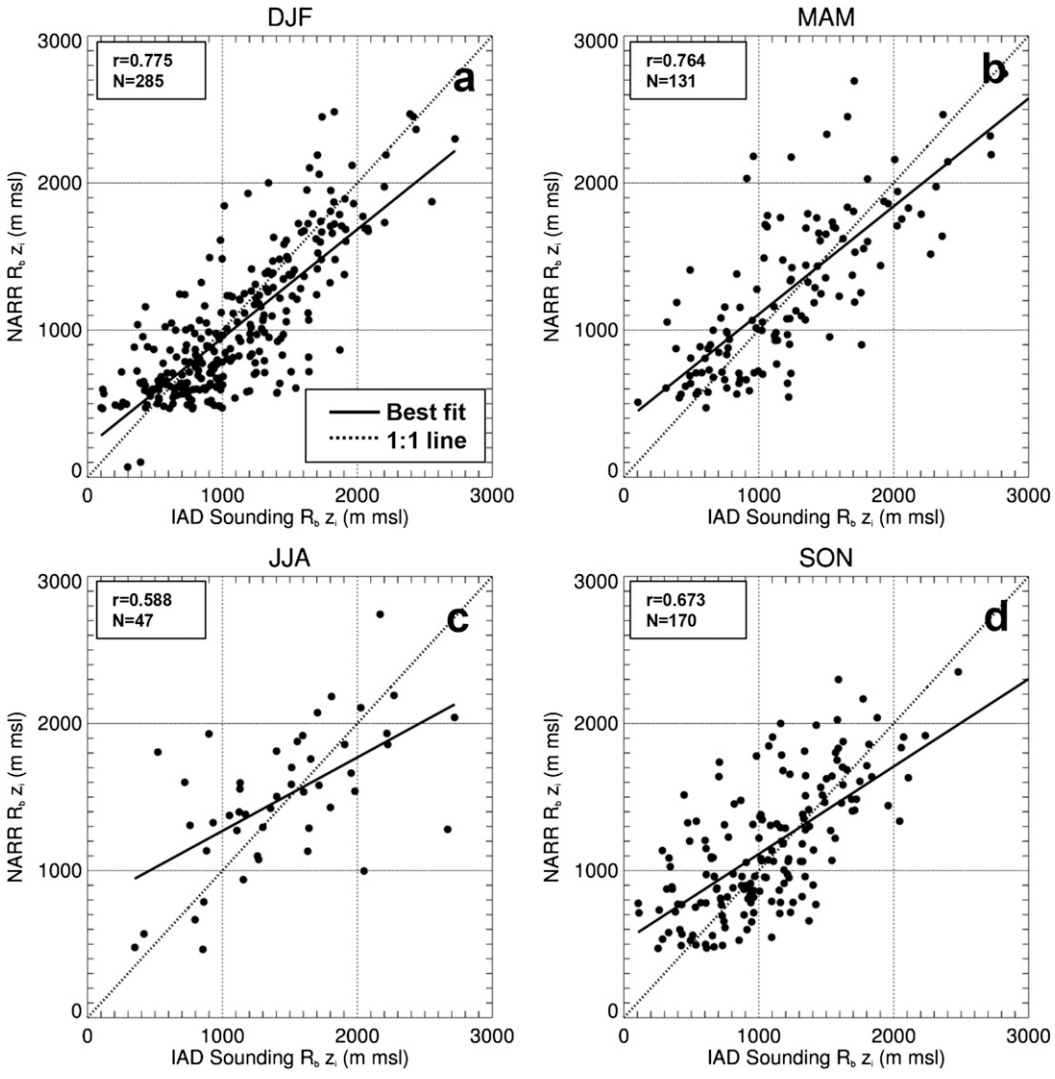


FIG. 4. Comparison between NARR and IAD rawinsonde PBL height for (a) winter, (b) spring, (c) summer, and (d) autumn for 1 Jan 2009–31 Dec 2012 for days in which PBL height is well defined. Dotted and solid lines indicate the 1:1 line and line of best fit, respectively. Pearson correlation coefficient $r$ and the number of cases $N$ are noted in the upper left of each figure. All correlations are significant at the 0.01 confidence level.

sporadic outliers in Fig. 4. The large differences occurred either on days on which there were multiple elevated stable layers or on days on which either the NARR or IAD-sounding $R_b$ profile slightly exceeded $R_c$ at a given height but the other profile did not.

We attempt to further remove days with large biases by removing cloudy days, on which the PBL height was oftentimes not well defined (e.g., Grimsdell and Angevine 1998), as well as windy days on which significant rawinsonde drift may occur (e.g., McGrath et al. 2006; Seidel et al. 2011). To this end, we identified clear or ''fair weather'' days using a clearness index. The clearness index (Whiteman et al. 1999) represents the ratio between the total amount of incoming solar radiation received at a given location summed for an entire day and the calculated maximum amount of incoming solar radiation that could be received at that location, following the method of Whiteman and Allwine (1986). We found no significant improvement of the relationship between the rawinsonde and NARR PBL height when we remove cloudy days (i.e., days with a clearness index $< 0.6$), days with rainfall, or days with 700-hPa wind speeds $> 15\,\mathrm{m\,s^{-1}}$.

From the above analyses, we conclude that removing days on which PBL height is poorly defined improves the relationship between the NARR PBL heights and IAD rawinsonde PBL heights. Days for which the differences exceed 1000 m still exist, however, which complicates a

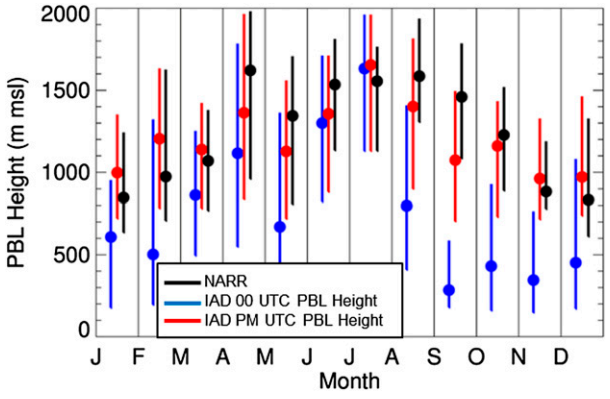


FIG. 5. Comparison between mean PBL height ± 1 standard deviation at IAD determined from the 0000 UTC IAD sounding (blue), 0000 UTC IAD sounding with the application of our afternoon PBL-height-detection approach (red), and 2100 UTC NARR PBL height at IAD (black) as a function of month over the period 1 Jan 2009–31 Dec 2012 for days on which the PBL height is well defined. All PBL heights are computed using the $R_b$ method. The offset within each month is to highlight the variability among the different methods.

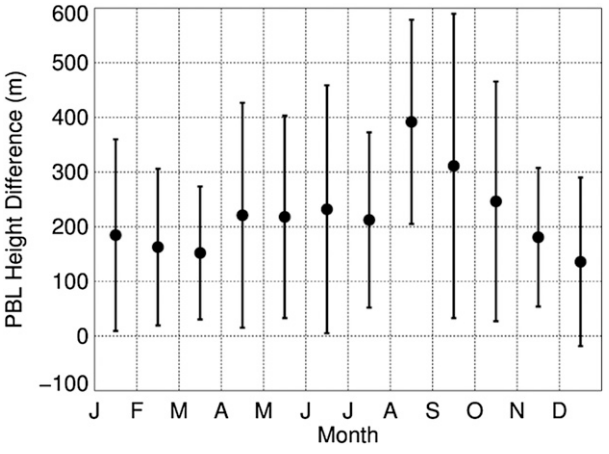


FIG. 6. Mean difference in 2100 UTC NARR PBL height ± 1 standard deviation between the Page Valley and IAD as a function of month for 1 Jan 2009–31 Dec 2012.

realistic estimation of PBL heights over the Page Valley on this subset of days. Thus, to provide the most reliable PBL-height estimates over the Page Valley from the IAD observations, we focus on days for which there is good agreement between NARR and IAD rawinsonde PBL height to understand the important physical processes governing the spatial PBL-height variability. Because there is good agreement between NARR and IAD rawinsonde PBL heights on monthly time scales (cf. Fig. 5), we use NARR to determine whether there are PBL-height differences between IAD and the Page Valley present on monthly time scales. We then use the higher-resolution WRF Model to investigate what additional physical processes are responsible for PBL-height differences on daily time scales to obtain the most reliable estimates of afternoon PBL heights over the Page Valley.

## 5. Results and discussion

### a. *Spatial PBL-height variability on monthly time scales*

To quantify PBL-height differences between IAD and the Page Valley, we calculated PBL height from NARR for the grid box containing IAD and the grid box containing SNP HQ and the Page Valley on the subset of days with well-defined PBL heights at IAD. We distinguish between the PBL height, which is the height of the PBL relative to sea level, and PBL depth, which is the height of the PBL relative to the underlying topography. Making this distinction is required to quantify the degree to which the PBL is affected by the underlying topography, which affects how well PBL-height observations from IAD can be used as a proxy for PBL heights over the Page Valley. For the 4-yr period of interest, there was good correlation between NARR PBL height at IAD and NARR PBL height over the Page Valley ($r = 0.94$; $p < 0.01$), and $r$ exceeded 0.9 in all seasons. PBL heights over the Page Valley were typically 200 m higher than at IAD during the winter and were nearly 400 m higher than at IAD in late summer (Fig. 6).

Important to consider, though, is the elevation difference between the NARR grid box containing the Page Valley and the grid box containing IAD. The IAD gridbox elevation is 115 m MSL, whereas the NARR grid box containing SNP HQ and Page Valley is 277 m MSL. Thus, the elevation difference between these two grid boxes is 162 m, which is comparable to the actual difference in elevation (~200 m). Thus, the differences in PBL height between the Page Valley and IAD imply that PBL depths were comparable in winter and ~200 m higher over the Page Valley than at IAD in the summer. Differentiating by PBL height with respect to the maximum ridgetop height (1200 m MSL), we found that PBL heights over the Page Valley were 218 ± 174 m higher than at IAD on days on which IAD PBL height is below the ridgetop height. On days on which IAD PBL height is above the ridgetop, the Page Valley PBL height was 157 ± 160 m higher than at IAD. Thus, spatial differences in PBL height tend to become smaller with an increase in PBL height as has been observed in other areas with mountainous terrain (De Wekker and Kossmann 2015). We observed a similar pattern when using other reanalysis and model products—that is, the

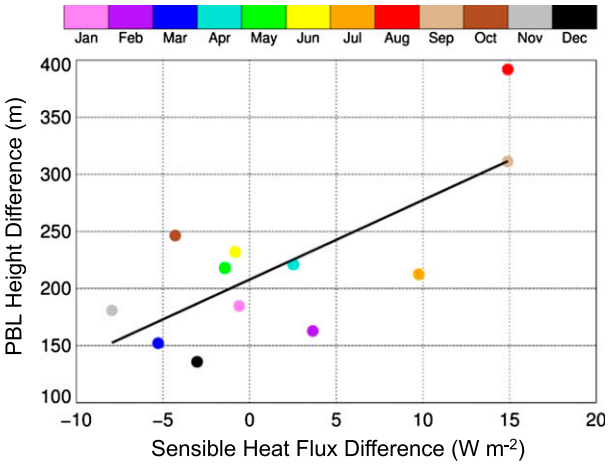


FIG. 7. Mean monthly difference between 2100 UTC PBL heights over the Page Valley and IAD as a function of the difference in mean monthly SHF between the Page Valley and IAD. Colored circles indicate different months; the black line indicates the line of best fit.

NAM and CFSR discussed in section 3e, implying that PBL-height differences between the Page Valley and IAD are not specific to NARR.

### b. *Drivers of PBL-height variability on monthly time scales*

From the analyses in the previous section, we conclude that PBL heights are typically higher over the Page Valley than near IAD, which is partly explained by the elevation difference of ~200 m. Summertime PBL-height differences are somewhat higher, and we hypothesize that this difference is caused by drier conditions over the Page Valley than at IAD that become more pronounced during the summer than during the winter. Drier conditions lead to more energy partitioned into SHF, resulting in deeper PBLs. To test this hypothesis, we used regional observations, NARR, and WRF simulations. Surface observations of afternoon SHF from monitoring sites within this region show a bimodal pattern during the year: one maximum occurs in April, and a secondary maximum occurs in late August and September (e.g., Lee et al. 2015). On the subset of days with well-defined PBL heights, NARR SHF differences between the Page Valley and IAD were positively correlated with PBL-height differences between the two locations ($r = 0.74$; $p < 0.01$) (Fig. 7). Furthermore, the precipitation differences between the Page Valley and IAD were largest in late summer and correlate with larger PBL-height differences ($r = -0.59$; $p = 0.04$). With less rainfall over the Page Valley, there was on average less soil moisture. Therefore, a greater percentage of incoming radiation was partitioned into SHF than into latent heat flux, yielding higher PBL heights over the Page Valley than near IAD. The differences in SHF between the Page Valley and IAD become largest in late summer when moisture differences are largest, resulting in the largest PBL-height differences during this time.

Thus, the higher PBL heights over the Page Valley are caused by higher terrain elevation and drier conditions that lead to larger SHF in the Page Valley than near IAD. We recognize that other factors may also play a role in causing day-to-day mesoscale PBL-height differences, including synoptic-scale subsidence and wind-flow patterns that are driven by the underlying topography (e.g., Kalthoff et al. 1998; Kossmann et al. 1998; Bianco et al. 2011). To investigate the potential role of subsidence, we compute mean monthly composites of vertical velocity (omega) in NARR for the same subset of days with well-defined PBL heights. Monthly NARR composites indicated smaller omega (i.e., less-positive values of omega and thus less subsidence) at 850 and 700 hPa during late summer over IAD than over the Page Valley (not shown), which would cause higher PBL heights at IAD than in the Page Valley. Because we typically observed higher PBL heights and PBL depths over the Page Valley, we conclude that synoptic-scale subsidence cannot explain PBL-height differences between the Page Valley and IAD on monthly time scales. To better understand large differences between NARR PBL heights and IAD rawinsonde PBL heights on daily time scales, we performed high-resolution WRF simulations as described in the next section.

### c. *Drivers of PBL-height variability on daily time scales*

Simulations were performed for 9 April 2009 and 23 October 2010, which were clear days for which rawinsonde observations were available from the Page Valley; these two days were characterized by deep PBLs and shallow PBLs, respectively. Details of the model evaluation are found in the appendix. Daytime near-surface temperatures in the region and the diurnal change in PBL height at IAD and in the Page Valley were simulated well on both days, providing us with confidence that our simulations could be used to further understand the PBL-height differences between IAD and the Page Valley. All simulations indicated that the PBL growth rate $dz_i/dt$ after sunrise was largest along the mountain ridges than in the valleys because of higher static stability in the valleys that suppresses PBL growth (Fig. 8a). Between 0800 and 1000 LST, the PBL height increased to 2000–2500 m MSL over the region on 9 April 2009 (Fig. 8b). During this time, $dz_i/dt$ was smaller over the eastern part of the domain than near

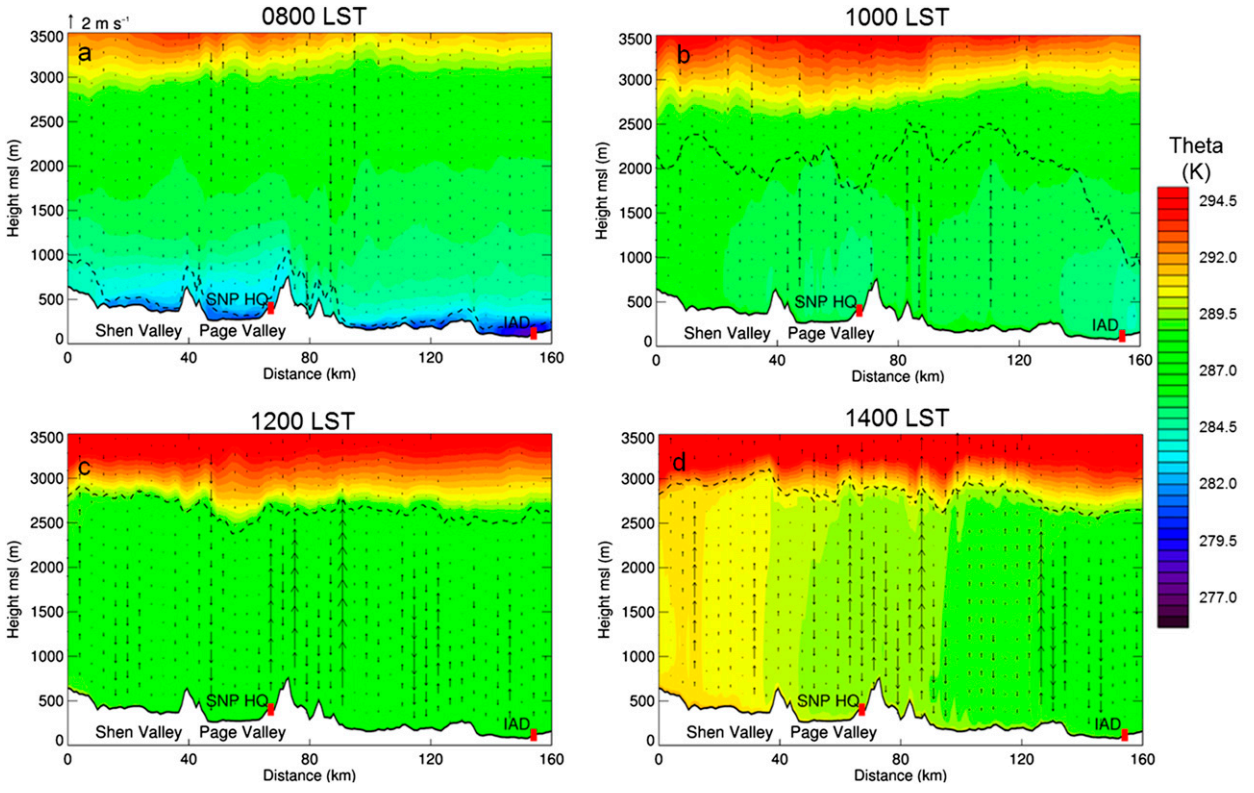


FIG. 8. Plots of $\theta$ cross section through SNP HQ (left red bar) and IAD (right red bar), shaded every 0.5 K, using WRF simulations with the YSU PBL scheme at (a) 0800, (b) 1000, (c) 1200, and (d) 1400 LST 9 Apr 2009. Arrows indicate vertical wind velocities. The dashed line indicates the PBL height computed using the $R_b$ method. The arrow at the top left of the figure indicates 2 m s$^{-1}$ vertical velocity. The locations of the Shenandoah and Page Valleys are indicated on the figure.

the Page Valley because of a deeper near-surface stable layer. By 1200 LST, the PBL height over the region ranged from approximately 2500 m MSL near IAD to 2900 m MSL over the Page and Shenandoah Valleys (Fig. 8c), and there was little additional increase in PBL height during the afternoon (Fig. 8d). On 23 October 2010, $dz_i/dt$ was much smaller than on 9 April 2009, and vertical velocities across the entire domain were weaker. Whereas vertical velocities exceeded 2 m s$^{-1}$ in the strongest updrafts during the afternoon on 9 April 2009, maximum vertical velocities on 23 October 2010 were ~0.75 m s$^{-1}$. On 23 October 2010, the PBL at 0800 LST was ~100 m deep across the ridges and <50 m in the valleys and east of the Blue Ridge Mountains (Fig. 9a). Between 0800 and 1200 LST, the PBL depth increased by approximately 500 m across the region (Figs. 9b,c) to a maximum of 600–800 m while generally following the underlying topography (Fig. 9d). As a consequence, there was more spatial PBL-height variability on 23 October 2010 than on 9 April 2009.

Despite the differences in afternoon PBL height on 9 April 2009 and 23 October 2010, a common feature of both days was the presence of higher PBL heights over the Page Valley than near IAD, which was consistent among simulations with four different PBL parameterization schemes and among different PBL-height determination methods. Higher PBL heights over the Page Valley than near IAD were also consistent with our findings from section 5a and with the rawinsonde observations made at both sites on these days.

We used our WRF simulations to investigate other causes of higher PBL heights over the Page Valley. Previous work has indicated that near-surface flow convergence can cause higher PBL heights over a valley head (Bianco et al. 2011). Following Bianco et al. (2011), we estimated convergence by calculating near-surface wind speed differences along the Page Valley using the model output. These analyses indicated no flow deceleration along the valley that would indicate convergence, either on 9 April 2009 or 23 October 2010. Furthermore, the simulations indicated that, consistent with the discussion in section 5b, higher PBL heights over the Page Valley could not be explained by subsidence differences. Instead, analyses of soil moisture in WRF provided further evidence that higher PBL heights over the Page Valley were partly due to

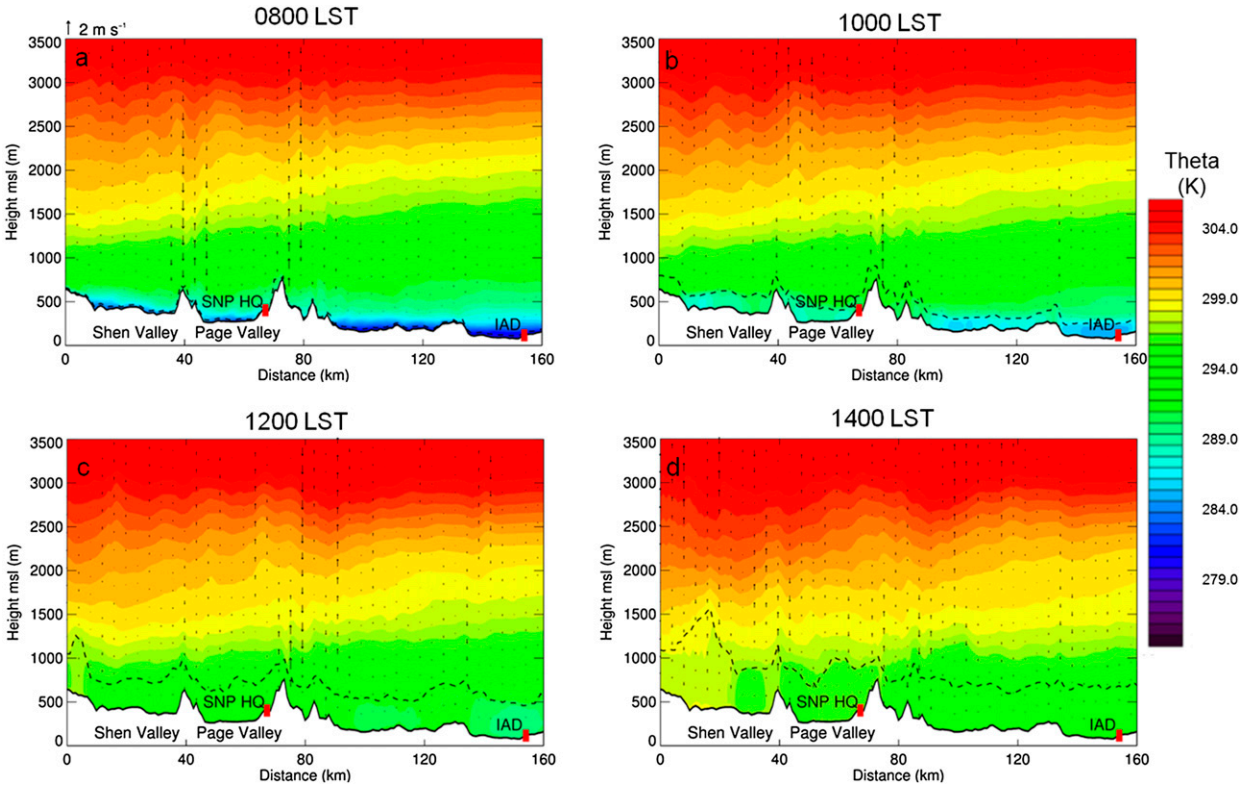


FIG. 9. As in Fig. 8, but for 23 Oct 2010; $\theta$ is shaded every 0.25 K.

differences in near-surface moisture. With drier conditions, there is higher SHF over the Page Valley than near IAD. For example, mean afternoon (1200–1600 LST) SHF on 9 April 2009 ranged from 339 to 407 W m$^{-2}$ at SNP HQ, depending on the PBL parameterization scheme used. At IAD, mean afternoon SHF for the four PBL parameterization schemes was consistently lower and ranged from 218 to 299 W m$^{-2}$. Further contributing to higher PBL heights over the western part of the domain and Page Valley could be the presence of a plain-to-mountain flow (e.g., Whiteman 2000) induced by the Blue Ridge Mountains acting as an elevated heat source. Although potential temperatures are about 2 K higher at a given height over the mountains than over the plains (cf. Figs. 8d and 9d), we find no evidence of this plain-to-mountain flow in either the simulations or regional observations, indicating that this circulation is too weak and/or is overwhelmed by the synoptic-scale flow.

Thus, our WRF simulations provide evidence that PBL-height and PBL-depth differences between IAD and the Page Valley are caused primarily by SHF and elevation differences between the two locations. To investigate to what extent the PBL height follows the topography, we computed the correlation between the PBL height and elevation for each grid point over the innermost domain (De Wekker 2002). A terrain-following PBL has a correlation coefficient $r$ of 1; the correlation for a non-terrain-following PBL is 0. Over the innermost WRF domain, $r$ exceeded 0.9 between 0000 and 0800 LST on both 9 April 2009 and 23 October 2010 (Fig. 10), indicating a terrain-following nighttime PBL on both days. At 0800 LST on 9 April 2009, $r$ initially decreased to a minimum of ~0.25 at 1100 LST but then increased to 0.6 during the midafternoon because of higher SHF over the western part of the domain that includes the Page and Shenandoah Valleys than over the eastern part of the domain that includes IAD. The correlation decreased during the daytime on both days, but the decrease was smaller on 23 October 2010 when $r$ remained above 0.75. A higher $r$ on 23 October 2010 indicated that the PBL more closely followed the terrain on this day than on 9 April 2009.

### d. *Estimating PBL heights over other areas in the study domain*

In summary, to use the 0000 UTC rawinsonde observations to estimate PBL heights over the Page Valley, we 1) computed PBL height from the IAD rawinsonde observations and NARR meteorological fields using the $R_b$ method, 2) removed the near-surface stable layer

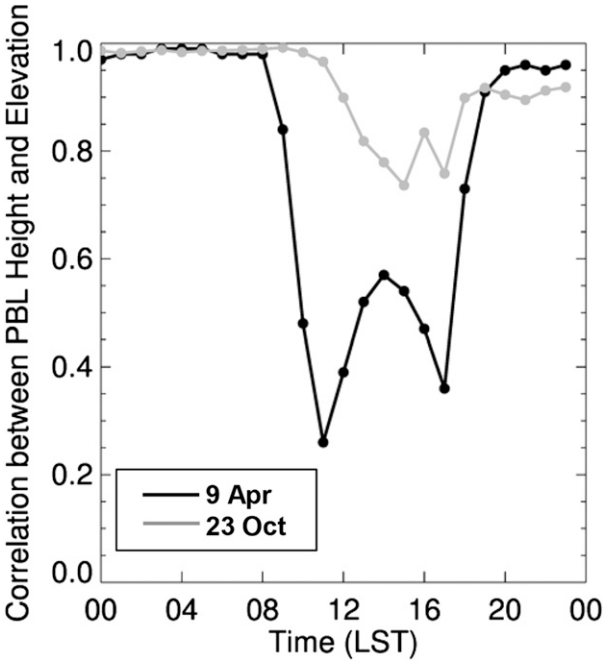


FIG. 10. Pearson correlation coefficient between PBL heights computed using the $R_b$ method and elevation over the innermost WRF domain for 9 Apr 2009 (black line) and 23 Oct 2010 (gray line).

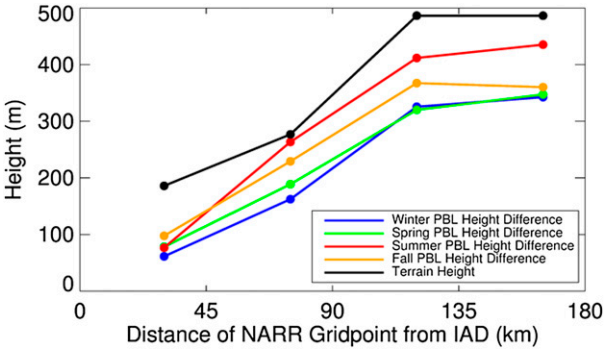


FIG. 11. Mean difference in NARR afternoon PBL height between the grid box containing IAD and PBL height along a transect extending from IAD southwestward through the Page and Shenandoah Valleys for winter (blue line), spring (green line), summer (red line), and autumn (orange line) for days with well-defined PBL heights at IAD. The black line shows the terrain height along the transect.

from the 0000 UTC IAD rawinsonde observations, and 3) selected days with well-defined PBL heights. Because there were still sometimes large differences between IAD rawinsonde PBL heights and NARR PBL heights on daily time scales (cf. Fig. 4), we conclude that NARR alone cannot provide the most reliable PBL height estimates over the Page Valley on daily time scales. Mean monthly NARR PBL heights calculated using the $R_b$ method, however, compared well to the mean monthly rawinsonde PBL height (cf. Fig. 5). Thus, combining NARR with rawinsonde PBL height can help to estimate PBL height at surrounding locations. Therefore, we used NARR to quantify regional PBL-height differences. To this end, we computed the mean difference between the NARR grid box containing IAD and the NARR grid boxes extending from IAD southwestward into the Page and Shenandoah Valleys. We found that mean PBL-height differences increase as a function of distance from IAD with an increase in terrain elevation (Fig. 11). PBL-height differences were largest in the summer when larger gradients in near-surface moisture exist and were smallest in winter. Consistent with results previously discussed (cf. Fig. 6), a location such as the Page Valley 100 km southwest of IAD has a PBL-height difference ranging from ~200 m in winter to ~350 m in summer. We note, though, that day-to-day PBL-height differences can be much larger or smaller, not only because of daily variability in soil moisture gradients (e.g., from localized rainfall events), but also because of advective effects that can affect the extent to which the PBL height follows the topography (e.g., De Wekker and Kossmann 2015).

## 6. Summary and conclusions

In this study, our goal was to estimate daytime maximum PBL height at certain locations using PBL height obtained from a nearby sounding station and from reanalysis products. We used the Page Valley in Virginia as a case study that has IAD as its nearest sounding station. We analyzed and evaluated reanalysis and model output for the region and investigated the processes responsible for the regional PBL-height spatiotemporal variability. Comparisons between rawinsonde and NARR PBL height showed low correlations that have also been reported in previous studies (e.g., Schmid and Niyogi 2012). Correlations between rawinsonde and NARR PBL heights improved when we recalculated the PBL height after removing the near-surface stable layer from the 0000 UTC $\theta_v$ profile and considered only cases in which the PBL height was well defined. Applying the approach of removing the near-surface stable layer to other regions where either 0000 or 1200 UTC is in the early evening will facilitate improved estimations of maximum daytime PBL height from rawinsonde observations, which are vital in air-quality and weather-forecasting applications.

We then quantified spatial PBL-height differences from NARR output and found that the PBL is typically 200–400 m higher over the Page Valley than at IAD,

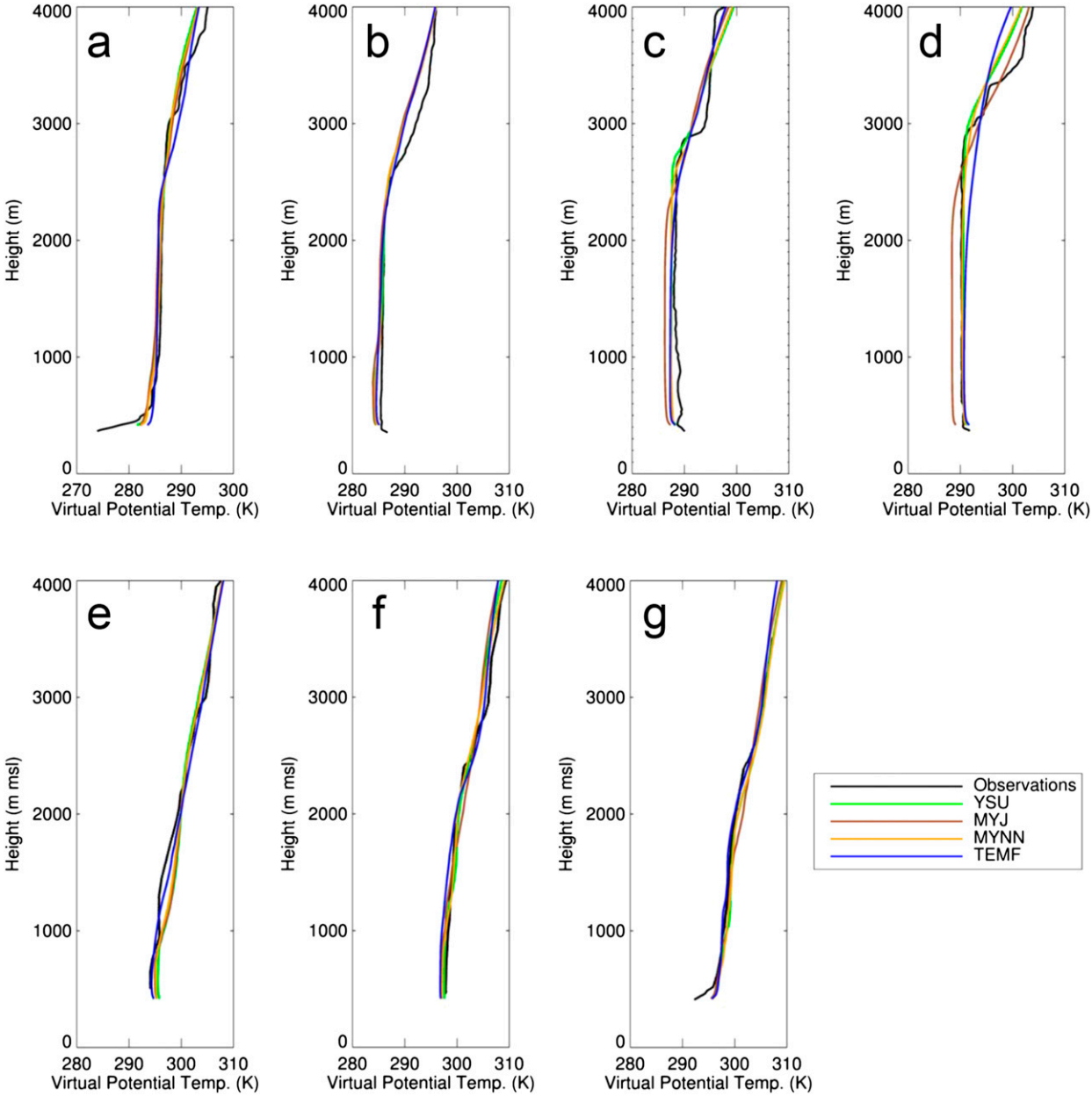


FIG. A1. Plots of $\theta_v$ profiles on 9 Apr 2009 at (a) 0600, (b) 0900, (c) 1200, and (d) 1500 LST and on 23 Oct 2010 at (e) 1300, (f) 1600, and (g) 1800 LST at SNP HQ from observations (black line) and using the YSU (green line), MYJ (brown line), MYNN2 (orange line), and TEMF (blue line) PBL schemes. The model output is the means over the nine model grid boxes surrounding SNP HQ. Note the different scales but the same range on the $x$ axis.

with somewhat smaller differences on days with deep PBLs. To understand the drivers responsible for the higher PBL heights over the Page Valley than at IAD, we performed WRF simulations. The simulations indicated that PBL heights exhibit terrain-following characteristics both on days with deep PBLs and days with shallow PBLs. Larger differences in the summertime can be explained by smaller soil moisture and larger SHF over the Page Valley than at IAD. These results were not sensitive to the choice of the PBL parameterization scheme in WRF.

From the WRF simulations and from the comparisons between the sounding observations and NARR, we conclude that adding the terrain-height difference between the Page Valley and IAD of ~200 m to the IAD PBL height yields a plausible estimate of the Page

TABLE A1. PBL heights (m MSL) at SNP HQ from the four soundings on 9 Apr 2009 and three soundings on 23 Oct 2010 (LST = UTC − 5 h), and model-derived PBL heights (m MSL) from four different PBL schemes. All PBL heights shown are computed using the $R_b$ method.

| Date | Time (LST) | SNP HQ | YSU | MYJ | MYNN2 | TEMF |
|---|---|---|---|---|---|---|
| 9 Apr 2009 | 0600 | 385 | 439 | 456 | 448 | 433 |
| | 0900 | 2386 | 1136 | 1165 | 1023 | 1472 |
| | 1200 | 2872 | 2754 | 2370 | 2586 | 2383 |
| | 1500 | 2971 | 3019 | 2443 | 2724 | 2341 |
| 23 Oct 2010 | 1300 | 730 | 907 | 847 | 822 | 910 |
| | 1600 | 669 | 1024 | 1012 | 802 | 983 |
| | 1800 | 363 | 453 | 449 | 448 | 450 |

Valley PBL height. Thus, to estimate the PBL height in different regions where PBL heights are unavailable, one could use rawinsonde observations from the nearest sounding station, assume that the PBL height follows the underlying terrain, and remove the elevation difference between the sounding station and the location of interest from the rawinsonde-derived PBL height. In a forthcoming study we use PBL-height estimates in the Page Valley from IAD PBL heights to investigate the impact of the valley PBL height relative to the mountaintop on the diurnal mountaintop trace-gas variability.

*Acknowledgments.* This research was partly funded by an MOU between the NOAA ESRL Global Monitoring Division and the University of Virginia, NOAA Award NA13OAR4310065, and NSF-CAREER Award ATM-1151445. We thank William Brown from the National Center for Atmospheric Research for conducting the rawinsonde launches at SNP HQ in April 2009 through an educational field deployment grant from the National Center for Atmospheric Research. We also thank the support of the undergraduate and graduate students from the spring 2009 and fall 2010 mountain meteorology courses taught at the University of Virginia. We thank John Kochendorfer and Maggie Robinson at the NOAA ARL Atmospheric Turbulence and Diffusion Division who helped improve the grammar in the manuscript. We also thank the three anonymous reviewers whose suggestions helped to improve the manuscript.

## APPENDIX

### WRF Evaluation

To have confidence in our WRF simulations, we focused on how well the different PBL parameterization schemes simulated daytime temperature and PBL evolution over the region. On 9 April 2009 at SNP HQ and IAD, the mean bias error (MBE) in afternoon 2-m temperatures between the observations and model was less than 1°C with the MYNN2 and YSU PBL schemes but was −2° and 4°C with the MYJ and TEMF schemes, respectively. Comparisons between the SNP HQ rawinsonde observations and simulations on 9 April 2009 showed good agreement (Fig. A1). Although differences in the $\theta_v$ profiles among the simulations varied by less than 2°C, the YSU scheme best simulated the $\theta_v$ profile and the PBL height (Table A1). On 23 October 2010, the simulations had a cool bias of 1°–2°C in the SNP HQ $\theta_v$ profile (Fig. A1). The simulations did not capture the near-surface stable layer that was present in the 1800 LST sounding but did capture the surface temperature decrease around this time. Despite these biases at SNP HQ, the simulations provided good estimates of afternoon PBL height at SNP HQ, with an MBE of <200 m for the different PBL schemes.

These findings on the sensitivity to different PBL schemes are consistent with previous work (e.g., Hu et al. 2012; Xie et al. 2013). Nonlocal PBL schemes—for example, the YSU scheme—better simulate nonlocal transport in the daytime PBL than do local schemes (e.g., Xie et al. 2013). Although the TEMF scheme is a nonlocal scheme, the TEMF scheme is more suitable for simulating stable and shallow, cloud-topped PBLs (e.g., Angevine et al. 2010). As a consequence, the TEMF scheme does a poorer job than the YSU scheme in simulating deep daytime convective PBLs. Whereas underestimates are larger with local schemes, modifications to the MYJ scheme that have been incorporated into the MYNN2 scheme improve the representation of vertical mixing in the daytime PBL (Nakanishi and Niino 2009) and yielded better agreement with the SNP HQ and IAD observations than did the MYJ scheme. From the sensitivity tests discussed here, we conclude that, while differences in maximum afternoon PBL height among the PBL parameterization schemes studied varied by 500 m, all simulations captured the daytime PBL evolution in the Page Valley and at IAD.

## REFERENCES


Aneja, V. P., S. Pal Arya, Y. Li, C. G. Murray, and T. L. Manuszak, 2000: Climatology of diurnal trends and vertical distribution of ozone in the atmospheric boundary layer in urban North Carolina. *J. Air Waste Manage*, **50**, 54–64, doi:10.1080/10473289.2000.10463984.

Angevine, W. M., H. Jiang, and R. Mauritsen, 2010: Performance of an eddy diffusivity–mass flux scheme for shallow cumulus boundary layers. *Mon. Wea. Rev.*, **138**, 2895–2912, doi:10.1175/2010MWR3142.1.

Avissar, R., and T. Schmidt, 1998: An evaluation of the scale at which ground-surface heat flux patchiness affects the convective boundary layer using large-eddy simulations. *J. Atmos. Sci.*, **55**, 2666–2689, doi:10.1175/1520-0469(1998)055<2666:AEOTSA>2.0.CO;2.

Bianco, L., I. V. Djalaova, C. W. King, and J. M. Wilczak, 2011: Diurnal evolution and annual variability of boundary-layer height and its correlation to other meteorological variables in California's Central Valley. *Bound.-Layer Meteor.*, **140**, 491–511, doi:10.1007/s10546-011-9622-4.

Blay-Carreras, E. D., and Coauthors, 2014: Role of the residual layer and large-scale subsidence on the development and evolution of the convective boundary layer. *Atmos. Chem. Phys.*, **14**, 4515–4530, doi:10.5194/acp-14-4515-2014.

Bohnenstengel, S. I., S. Evans, P. A. Clark, and S. E. Belcher, 2011: Simulations of the London urban heat island. *Quart. J. Roy. Meteor. Soc.*, **137**, 1625–1640, doi:10.1002/qj.855.

Clifford, S. F., J. C. Kaimal, R. J. Lataitis, and R. G. Strauch, 1994: Ground-based remote profiling in atmospheric studies: An overview. *Proc. IEEE*, **82**, 313–355, doi:10.1109/5.272138.

Cressie, N. A. C., 1993: *Statistics for Spatial Data.* John Wiley and Sons, 900 pp.

Dabberdt, W. F., and Coauthors, 2004: Meteorological research needs for improved air quality forecasting: Report of the 11th prospectus development team of the U.S. Weather Research Program. *Bull. Amer. Meteor. Soc.*, **85**, 563–586, doi:10.1175/BAMS-85-4-563.

Davis, R. E., C. P. Normile, L. Sitka, D. M. Hondula, D. B. Knight, S. P. Gawtry, and P. J. Stenger, 2010: A comparison of trajectory and air mass approaches to examine ozone variability. *Atmos. Environ.*, **44**, 64–74, doi:10.1016/j.atmosenv.2009.09.038.

Desai, A. R., K. J. Davis, C. J. Senff, S. Ismail, E. V. Browell, D. R. Stauffer, and B. P. Reen, 2006: A case study on the effects of heterogeneous soil moisture on mesoscale boundary-layer structure in the southern Great Plains, U.S.A. Part I: Simple prognostic model. *Bound.-Layer Meteor.*, **119**, 195–238, doi:10.1007/s10546-005-9024-6.

De Wekker, S. F. J., 2002: Structure and morphology of the convective boundary layer in mountainous terrain. Ph.D. dissertation, University of British Columbia, 191 pp.

——, and M. Kossmann, 2015: Convective boundary layer heights over mountainous terrain—A review of concepts. *Front. Earth Sci.*, **3**, doi:10.3389/feart.2015.00077.

Drüe, C., T. Hauf, and A. Hoff, 2010: Comparison of boundary-layer profiles and layer detection by AMDAR and WTR/RASS at Frankfurt Airport. *Bound.-Layer Meteor.*, **135**, 407–432, doi:10.1007/s10546-010-9485-0.

Dudhia, J., 1989: Numerical study of convection observed during the winter monsoon experiment using a mesoscale two-dimensional model. *J. Atmos. Sci.*, **46**, 3077–3107, doi:10.1175/1520-0469(1989)046<3077:NSOCOD>2.0.CO;2.

Elansky, N. F., M. A. Lokoshchenko, I. B. Belikov, A. I. Skorokhod, and R. A. Shumskii, 2007: Variability of trace gases in the atmospheric boundary layer from observations in the city of Moscow. *Atmos. Ocean. Phys.*, **43**, 219–231, doi:10.1134/S0001433807020089.

Grimsdell, A. W., and W. M. Angevine, 1998: Convective boundary layer height measurement with wind profilers and comparison to cloud base. *J. Atmos. Oceanic Technol.*, **15**, 1331–1338, doi:10.1175/1520-0426(1998)015<1331:CBLHMW>2.0.CO;2.

Holzworth, G. C., 1964: Estimates of mean maximum mixing depths in the contiguous United States. *Mon. Wea. Rev.*, **92**, 235–242, doi:10.1175/1520-0493(1964)092<0235:EOMMMD>2.3.CO;2.

Hondula, D. M., and Coauthors, 2013: A respiratory alert model for the Shenandoah Valley, Virginia, USA. *Int. J. Biometeor.*, **57**, 91–105, doi:10.1007/s00484-012-0537-7.

Hong, S. Y., J. Dudhia, and S. H. Chen, 2004: A revised approach to ice microphysical processes for the bulk parameterization of clouds and precipitation. *Mon. Wea. Rev.*, **132**, 103–120, doi:10.1175/1520-0493(2004)132<0103:ARATIM>2.0.CO;2.

——, Y. Noh, and J. Dudhia, 2006: A new vertical diffusion package with an explicit treatment of entrainment processes. *Mon. Wea. Rev.*, **134**, 2318–2341, doi:10.1175/MWR3199.1.

Horel, J., and Coauthors, 2002: Mesowest: Cooperative mesonets in the western United States. *Bull. Amer. Meteor. Soc.*, **83**, 211–225, doi:10.1175/1520-0477(2002)083<0211:MCMITW>2.3.CO;2.

Hu, X. M., D. C. Doughty, K. J. Sanchez, E. Joseph, and J. D. Fuentes, 2012: Ozone variability in the atmospheric boundary layer in Maryland and its implications for vertical transport model. *Atmos. Environ.*, **46**, 354–364, doi:10.1016/j.atmosenv.2011.09.054.

Janjić, Z. I., 1990: The step-mountain coordinate: Physical package. *Mon. Wea. Rev.*, **118**, 1429–1443, doi:10.1175/1520-0493(1990)118<1429:TSMCPP>2.0.CO;2.

Jordan, N. S., R. M. Hoff, and J. Bacmeister, 2010: Validation of Goddard Earth Observing System-version 5 MERRA planetary boundary layer heights using *CALIPSO*. *J. Geophys. Res.*, **115**, D24218, doi:10.1029/2009JD013777.

Kain, J. S., and J. M. Fritsch, 1990: A one-dimensional entraining/detraining plume model and its application in convective parameterization. *J. Atmos. Sci.*, **47**, 2784–2802, doi:10.1175/1520-0469(1990)047<2784:AODEPM>2.0.CO;2.

Kalthoff, N., H.-J. Binder, M. Kossmann, R. Vögtlin, U. Corsmeier, F. Fiedler, and H. Schlager, 1998: Temporal evolution and spatial variation of the boundary layer over complex terrain. *Atmos. Environ.*, **32**, 1179–1194, doi:10.1016/S1352-2310(97)00193-3.

Ketterer, C., P. Zieger, N. Bukowiecki, M. Collaud Coen, O. Maier, D. Ruffieux, and E. Weingartner, 2014: Investigation of the planetary boundary layer in the Swiss Alps using remote sensing and in situ measurements. *Bound.-Layer Meteor.*, **151**, 317–334, doi:10.1007/s10546-013-9897-8.

Korhonen, K., and Coauthors, 2014: Atmospheric boundary layer top height in South Africa: Measurements with lidar and radiosonde compared to three atmospheric models. *Atmos. Chem. Phys.*, **14**, 4263–4278, doi:10.5194/acp-14-4263-2014.

Kossmann, M., R. Vögtlin, U. Corsmeier, B. Vogel, F. Fiedler, H.-J. Binder, N. Kalthoff, and F. Beyrich, 1998: Aspects of the convective boundary layer structure over complex terrain. *Atmos. Environ.*, **32**, 1323–1348, doi:10.1016/S1352-2310(97)00271-9.

Kretschmer, R., F. Koch, D. Feist, G. Biavati, U. Karstens, and C. Gerbig, 2013: Toward assimilation of observation-derived mixing heights to improve atmospheric tracer transport models. *Lagrangian Modeling of the Atmosphere*, J. Lin et al., Eds., Amer. Geophys. Union, doi:10.1029/2012GM001255.

——, C. Gerbig, U. Karstens, G. Biavati, A. Vermeulen, F. Vogel, S. Hammer, and K. U. Totsche, 2014: Impact of optimized mixing heights on simulated regional atmospheric transport of $CO_2$. *Atmos. Chem. Phys.*, **14**, 7149–7172, doi:10.5194/acp-14-7149-2014.

Lee, T. R., 2015: The impact of planetary boundary layer dynamics on mountaintop trace gas variability. Ph.D. dissertation, University of Virginia, 213 pp.

——, S. F. J. De Wekker, A. E. Andrews, J. Kofler, and J. Williams, 2012: Carbon dioxide variability during cold front passages and fair weather days at a forested mountaintop site. *Atmos. Environ.*, **46**, 405–416, doi:10.1016/j.atmosenv.2011.09.068.

——, ——, and J. E. B. Wofford, 2014a: Downscaling maximum temperature projections to subkilometer resolutions in the Shenandoah National Park of Virginia, USA. *Adv. Meteor.*, 594965, doi:10.1155/2014/594965.

——, ——, and ——, 2014b: Downscaling temperatures to Shenandoah National Park using gridded climate data sets, high-resolution atmospheric models, and surface observations: Final report in completion of cooperative agreement 484010004. National Park Service Natural Resource Tech. Rep. NPS/SHEN/NRTR—2014/875, 96 pp. [Available online at http://irmafiles.nps.gov/reference/holding/495974.]

——, ——, S. Pal, A. E. Andrews, and J. Kofler, 2015: Meteorological controls on the diurnal variability of carbon monoxide mixing ratio at a mountaintop monitoring site in the Appalachian Mountains. *Tellus*, **67B**, 25659, doi:10.3402/tellusb.v67.25659.

Liu, S., and X.-Z. Liang, 2010: Observed diurnal cycle climatology of planetary boundary layer height. *J. Climate*, **23**, 5790–5809, doi:10.1175/2010JCLI3552.1.

Ma, M., Z. Pu, S. Wang, and Q. Zhang, 2011: Characteristics and numerical simulations of extremely large atmospheric boundary-layer heights over an arid region in north-west China. *Bound.-Layer Meteor.*, **140**, 163–176, doi:10.1007/s10546-011-9608-2.

McGrath, R., T. Semmler, S. Sweeney, and S. Wang, 2006: Impact of balloon drift errors in radiosonde data on climate statistics. *J. Climate*, **19**, 3430–3442, doi:10.1175/JCLI3804.1.

Menut, L., C. Flamant, J. Pelon, and P. H. Flamant, 1999: Urban boundary-layer height determination from lidar measurements over the Paris area. *Appl. Opt.*, **38**, 945–954, doi:10.1364/AO.38.000945.

Mesinger, F., and Coauthors, 2006: North American Regional Reanalysis. *Bull. Amer. Meteor. Soc.*, **87**, 343–360, doi:10.1175/BAMS-87-3-343.

Mlawer, E. J., S. J. Taubman, P. D. Brown, M. J. Iacono, and S. A. Clough, 1997: Radiative transfer for inhomogeneous atmospheres: RRTM, a validated correlated-*k* model for the longwave. *J. Geophys. Res.*, **102**, 16 663–16 682, doi:10.1029/97JD00237.

Nakanishi, M., and H. Niino, 2009: Development of an improved turbulence closure model for the atmospheric boundary layer. *J. Meteor. Soc. Japan*, **87**, 895–912, doi:10.2151/jmsj.87.895.

Nyeki, S., and Coauthors, 2000: Convective boundary layer evolution to 4 km ASL over high-alpine terrain: Airborne lidar observations in the Alps. *Geophys. Res. Lett.*, **27**, 689–692, doi:10.1029/1999GL010928.

Olson, J., and G. Grell, 2014: Improving the Rapid Refresh and High Resolution Rapid Refresh physics to better perform across a wide range of spatial scales. *Geophys. Res. Abstracts*, **16**, 7816. [Available online at http://meetingorganizer.copernicus.org/EGU2014/EGU2014-7816.pdf.]

Pal, S., T. R. Lee, S. Phelps, and S. F. J. De Wekker, 2014: Impact of atmospheric boundary layer depth variability and wind reversal on the diurnal variability of aerosol concentration at a valley site. *Sci. Total Environ.*, **496**, 424–434, doi:10.1016/j.scitotenv.2014.07.067.

Pochanart, P., H. Akimoto, Y. Kajii, and P. Sukasem, 2003: Carbon monoxide, regional-scale transport, and biomass burning in tropical continental Southeast Asia: Observations in rural Thailand. *J. Geophys. Res.*, **108**, 4552, doi:10.1029/2002JD003360.

Popa, M. E., M. Gloor, A. C. Manning, A. Jordan, U. Schultz, F. Haensel, T. Seifert, and M. Heimann, 2010: Measurements of greenhouse gases and related tracers at Bialystok tall tower station in Poland. *Atmos. Meas. Tech.*, **3**, 407–427, doi:10.5194/amt-3-407-2010.

Raatikainen, T., A.-P. Hyvärinen, J. Hatakka, T. S. Panwar, R. K. Hooda, V. P. Sharma, and H. Lihavainen, 2014: The effect of boundary layer dynamics on aerosol properties at the Indo-Gangetic plains and at the foothills of the Himalayas. *Atmos. Environ.*, **89**, 548–555, doi:10.1016/j.atmosenv.2014.02.058.

Saha, S., and Coauthors, 2010: The NCEP Climate Forecast System Reanalysis. *Bull. Amer. Meteor. Soc.*, **91**, 1015–1057, doi:10.1175/2010BAMS3001.1.

Sahu, L. K., Y. Kondo, Y. Miyazaki, P. Pongkiatkul, and N. T. K. Oanh, 2011: Seasonal and diurnal variations of black carbon and organic carbon aerosols in Bangkok. *J. Geophys. Res.*, **116**, D15302, doi:10.1029/2010JD015563.

Schmid, P., and D. Niyogi, 2012: A method for estimating planetary boundary layer heights and its application over the ARM Southern Great Plains site. *J. Atmos. Oceanic Technol.*, **29**, 316–322, doi:10.1175/JTECH-D-11-00118.1.

Segal, M., R. Avissar, M. C. McCumber, and R. A. Pielke, 1988: Evaluation of vegetation effects on the generation and modification of mesoscale circulations. *J. Atmos. Sci.*, **45**, 2268–2292, doi:10.1175/1520-0469(1988)045<2268:EOVEOT>2.0.CO;2.

Seibert, P., F. Beyrich, S.-E. Gryning, S. Joffre, A. Rasmussen, and P. Tercier, 2000: Review and intercomparison of operational methods for the determination of the mixing height. *Atmos. Environ.*, **34**, 1001–1027, doi:10.1016/S1352-2310(99)00349-0.

Seidel, D. J., C. A. Ao, and K. Li, 2010: Estimating climatological planetary boundary layer heights from radiosonde observations: Comparison of methods and uncertainty analysis. *J. Geophys. Res.*, **115**, D16113, doi:10.1029/2009JD013680.

——, B. Sun, M. Pettey, and A. Reale, 2011: Global radiosonde balloon drift statistics. *J. Geophys. Res.*, **116**, D07102, doi:10.1029/2010JD014891.

——, Y. Zhang, A. Beljaars, J.-C. Golaz, A. R. Jacobson, and B. Medeiros, 2012: Climatology of the planetary boundary layer over the continental United States and Europe. *J. Geophys. Res.*, **117**, D17106, doi:10.1029/2012JD018143.

Skamarock, W. C., and Coauthors, 2008: A description of the Advanced Research WRF version 3. NCAR Tech. Note NCAR/TN-475+STR, 113 pp., doi:10.5065/D68S4MVH.

Stull, R. B., 1988: *An Introduction to Boundary Layer Meteorology.* Kluwer Academic, 666 pp.

Sun, W.-Y., and Y. Ogura, 1980: Modeling the evolution of the convective planetary boundary layer. *J. Atmos. Sci.*, **37**, 1558–1572, doi:10.1175/1520-0469(1980)037<1558:MTEOTC>2.0.CO;2.

Vogelezang, D. H. P., and A. A. M. Holtslag, 1996: Evaluation and model impacts of alternative boundary-layer height formulations. *Bound.-Layer Meteor.*, **81**, 245–269, doi:10.1007/BF02430331.

Volz-Thomas, A., H.-W. Patz, N. Houben, S. Konrad, D. Mihelcic, T. Klüpfel, and D. Perner, 2003: Inorganic trace gases and peroxy radicals during BERLIOZ at Pabstthum: An investigation of the photostationary state of $NO_x$ and $O_3$. *J. Geophys. Res.*, **108**, 8248, doi:10.1029/2001JD001255.

von Engeln, A., and J. Teixeira, 2013: A planetary boundary layer height climatology derived from ECMWF reanalysis data. *J. Climate*, **26**, 6575–6590, doi:10.1175/JCLI-D-12-00385.1.

——, G. Nedoluha, and J. Teixeira, 2003: An analysis of the frequency and distribution of ducting events in simulated radio occultation measurements based on ECMWF fields. *J. Geophys. Res.*, **108**, 4669, doi:10.1029/2002JD003170.

Wang, X. Y., and K. C. Wang, 2014: Estimation of atmospheric mixing layer height from radiosonde data. *Atmos. Meas. Tech.*, **7**, 1701–1709, doi:10.5194/amt-7-1701-2014.

Whiteman, C. D., 2000: *Mountain Meteorology: Fundamentals and Applications*. Oxford University Press, 355 pp.

——, and K. J. Allwine, 1986: Extraterrestrial solar radiation on inclined surfaces. *Environ. Software*, **1** (3), 164–169, doi:10.1016/0266-9838(86)90020-1.

——, X. Bian, and S. Zhong, 1999: Wintertime evolution of the temperature inversion in the Colorado Plateau Basin. *J. Appl. Meteor.*, **38**, 1103–1117, doi:10.1175/1520-0450(1999)038<1103:WEOTTI>2.0.CO;2.

Winker, D. M., W. H. Hunt, and M. J. McGill, 2007: Initial performance assessment of CALIOP. *Geophys. Res. Lett.*, **34**, L19803, doi:10.1029/2007GL030135.

Xie, B., J. C. H. Fung, A. Chan, and A. Lau, 2012: Evaluation of nonlocal and local planetary boundary layer schemes in the WRF model. *J. Geophys. Res.*, **117**, D12103, doi:10.1029/2011JD017080.

——, J. C. R. Hunt, D. J. Carruthers, J. C. H. Fung, and J. F. Barlow, 2013: Structure of the planetary boundary layer over southeast England: Modeling and measurements. *J. Geophys. Res. Atmos.*, **118**, 7799–7818, doi:10.1002/jgrd.50621.

Xiu, A., and J. E. Pleim, 2001: Development of a land surface model. Part I: Application in a mesoscale meteorological model. *J. Appl. Meteor.*, **40**, 192–209, doi:10.1175/1520-0450(2001)040<0192:DOALSM>2.0.CO;2.

Yver, C. E., H. D. Graven, D. D. Lucas, P. J. Cameron-Smith, R. F. Keeling, and R. F. Weiss, 2013: Evaluating transport in the WRF Model along the California coast. *Atmos. Chem. Phys.*, **13**, 1837–1852, doi:10.5194/acp-13-1837-2013.

Zhang, Y., Z. Gao, D. Li, Y. Li, N. Zhang, X. Zhao, and J. Chen, 2014: On the computation of planetary boundary layer height using the bulk Richardson number method. *Geosci. Model Dev.*, **7**, 2599–2611, doi:10.5194/gmd-7-2599-2014.

Zhong, S., and F. K. Chow, 2013: Meso- and fine-scale modeling over complex terrain: Parameterizations and applications. *Mountain Weather Research and Forecasting: Recent Progress and Current Challenges*, F. K. Chow, S. F. J. De Wekker, and B. J. Snyder, Eds., Springer, 591–654.